

Filo del Sol Alteration Report

Alteration Mapping Using WorldView-3
Satellite Imagery and Spectral Matching
with Deep Learning Algorithms

Authors:

Margaret McPherson, P.Geo.

Kieran Kristoffersen, G.I.T.



Contact Information

Head Office

PhotoSat Information Ltd.

#580—1188 West Georgia Street

Vancouver BC V6A 4E2

1-604-681-9770 | info@photosat.ca

Authors

Margaret McPherson, P. Geo.

Senior Alteration Analyst

margaret.mcpherson@photosat.ca

Kieran Kristoffersen, G.I.T.

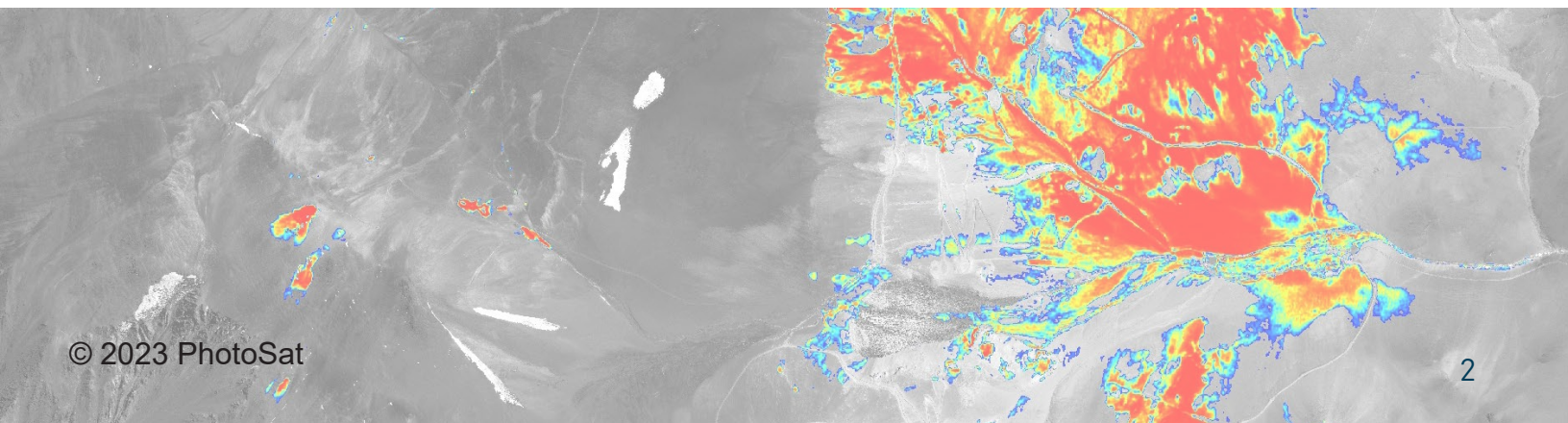
Geology Analyst

kieran.kristoffersen@photosat.ca

Date of Publication

First: January 1st, 2021

Revised: March 12th, 2023



Contents

Abstract	6
Introduction	7
Filo del Sol Deposit	7
Methods	8
Spectral Matching	9
Deep Learning	10
Results	11
Discussion	29

List of Figures

Figure 1: Location of the Filo del Sol deposit	6
Figure 2: Close-up of kaolinite at the Filo del Sol Zone	7
Figure 3: Bands detected by WV-3 and ASTER	8
Figure 4: SWIR pixel size of WV-3 and ASTER	8
Figure 5a: Spectral profile of kaolinite with WV-3	9
Figure 5b: Spectral profile of alunite with WV-3	9
Figure 6: Natural colour image of the Filo del Sol deposit	11
Figure 7: Geology enhanced image of the Filo del Sol deposit	12
Figure 8: Alteration map of alunite with WV-3 imagery	13
Figure 9: Alteration map of kaolinite with WV-3 imagery	14
Figure 10: Alteration map of buddingtonite with WV-3 imagery	15
Figure 11: Alteration map of opal/chalcedony with WV-3 imagery	16
Figure 12: Alteration map of calcite with WV-3 imagery	17
Figure 13: Alteration map of chlorite/epidote with WV-3 imagery	18
Figure 14: Alteration map of sericite with WV-3 imagery	19
Figure 15: Alteration map of montmorillonite with WV-3 imagery	20
Figure 16: Alteration map of goethite with WV-3 imagery	21
Figure 17: Alteration map of hematite with WV-3 imagery	22

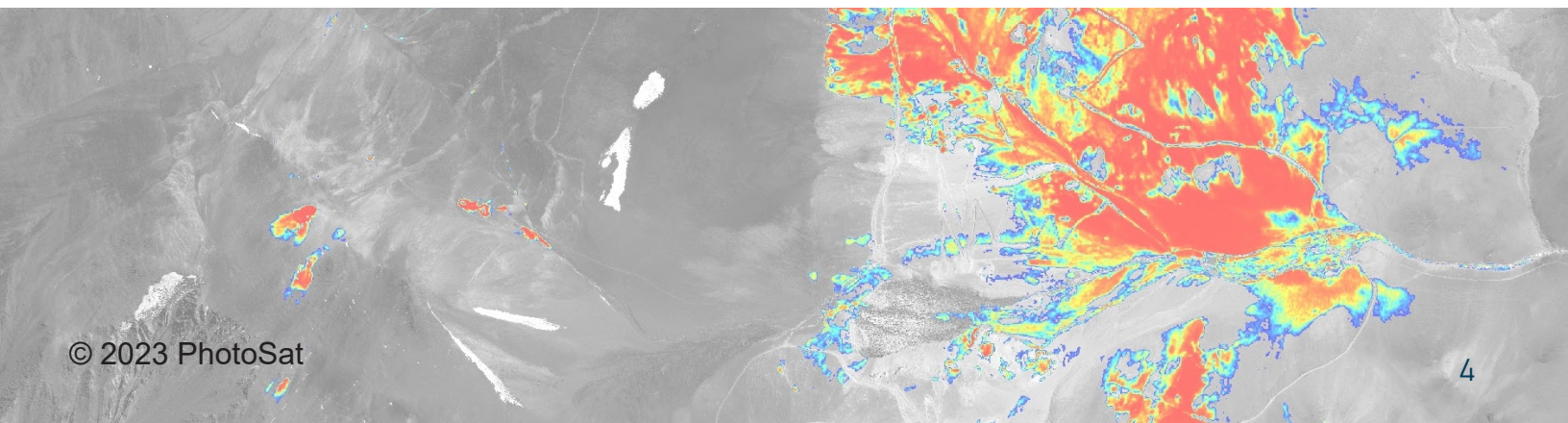


Figure 18: Alteration map of jarosite with WV-3 imagery 23

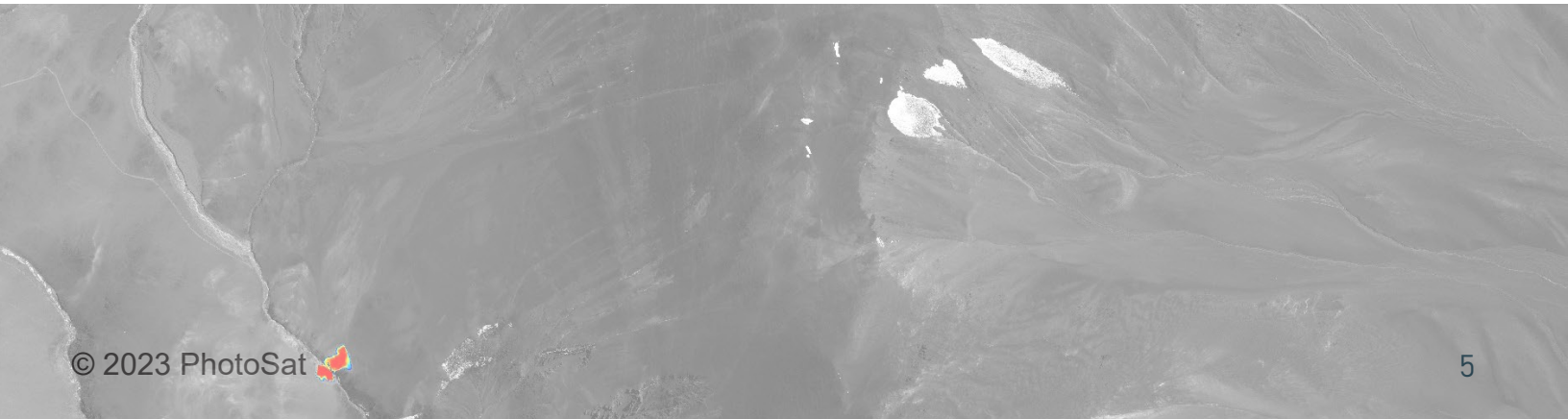
Figure 19: Alteration map of iron oxide gossans with WV-3 imagery 24

Figure 20: Alteration map of silica (75 m) from ASTER imagery 25

Figure 21: Compilation map of clays and other minerals 26

Figure 22: Compilation map of micas, clays, and other minerals 27

Figure 23: Compilation map of iron minerals 28



Abstract

The Filo del Sol project has been explored by Filo Mining Corp, or its predecessors, since 1999.

It is located in the San Juan Province of Argentina and the adjacent Atacama Region of Northern Chile, 140 kilometres southeast of the city of Copiapó, Chile, and straddles the border between Argentina and Chile.

Filo del Sol is a high-sulphidation epithermal copper-gold-silver deposit, associated with a large porphyry copper-gold system.

In this alteration report, PhotoSat produces a series of alteration mineral maps from WorldView-3 satellite imagery and archive ASTER satellite imagery for the area around the Filo del Sol deposit.

As part of Filo Mining's 2021 exploration program, drill core samples confirmed the presence of high-grade copper, gold, and silver. Photosat's satellite alteration mapping results show a correlation between these known mineralized zones and the local distribution of key alteration minerals.

For results, read the full alteration report.

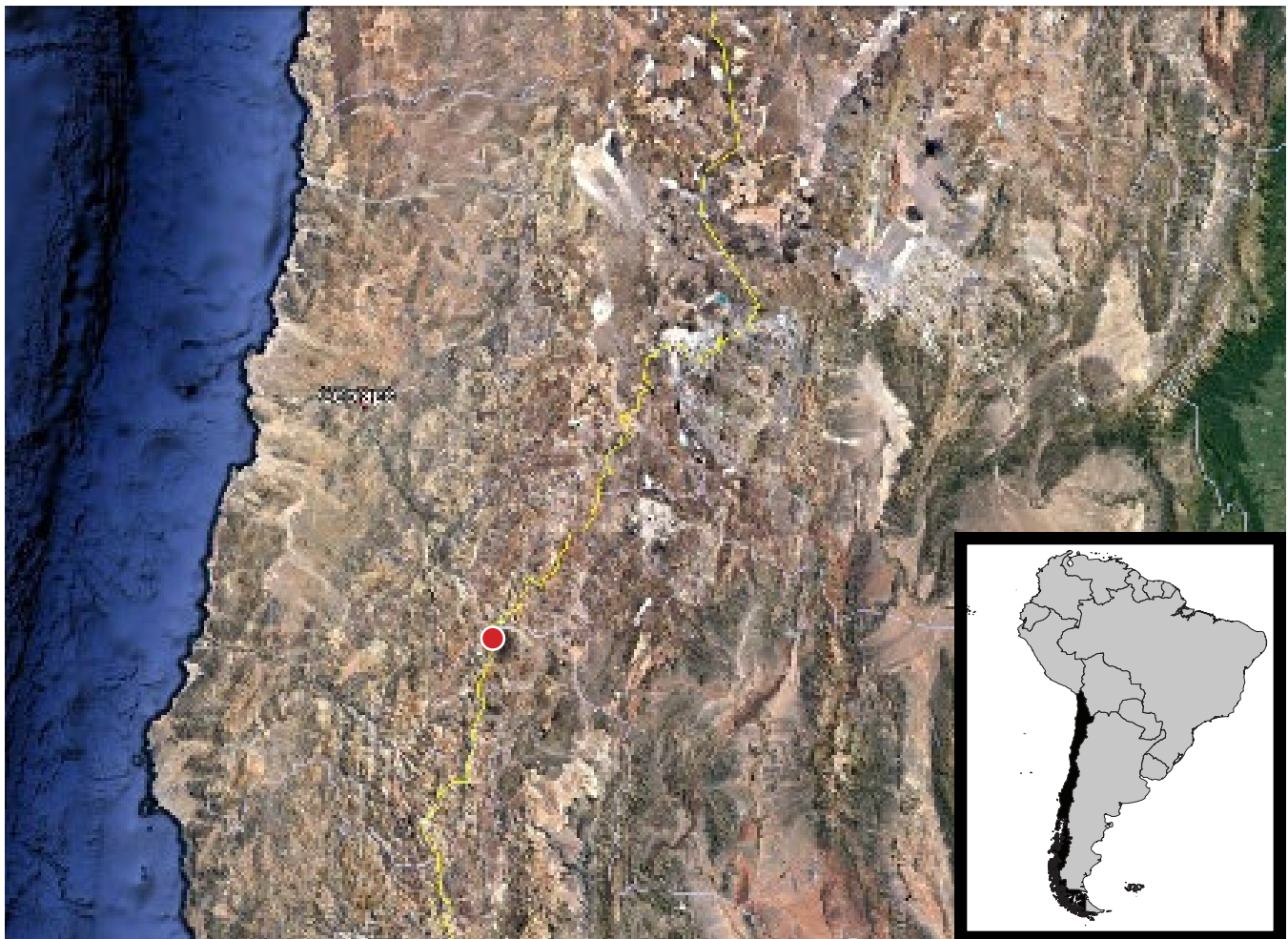


Figure 1: Location of the Filo del Sol deposit

Introduction

This report details the WorldView-3 satellite alteration mineral mapping results for the Filo del Sol Deposit.

Filo del Sol Deposit

Filo del Sol is a high-sulphidation epithermal copper-gold-silver deposit associated with a large porphyry copper-gold system.

Overlapping mineralizing events combined with weathering effects, including supergene enrichment, have created

several different styles of mineralization, including structurally-controlled and breccia-hosted gold, manto-style high-grade silver (+/- copper) and high-grade supergene enriched copper within a broader envelope of disseminated, stockwork and breccia-hosted sulphide copper and gold mineralization.

This complex geological history has created a heterogeneous orebody which is characterized by zones of very high-grade copper +/- gold +/- silver mineralization within a large envelope of more homogeneous, lower-grade mineralization.

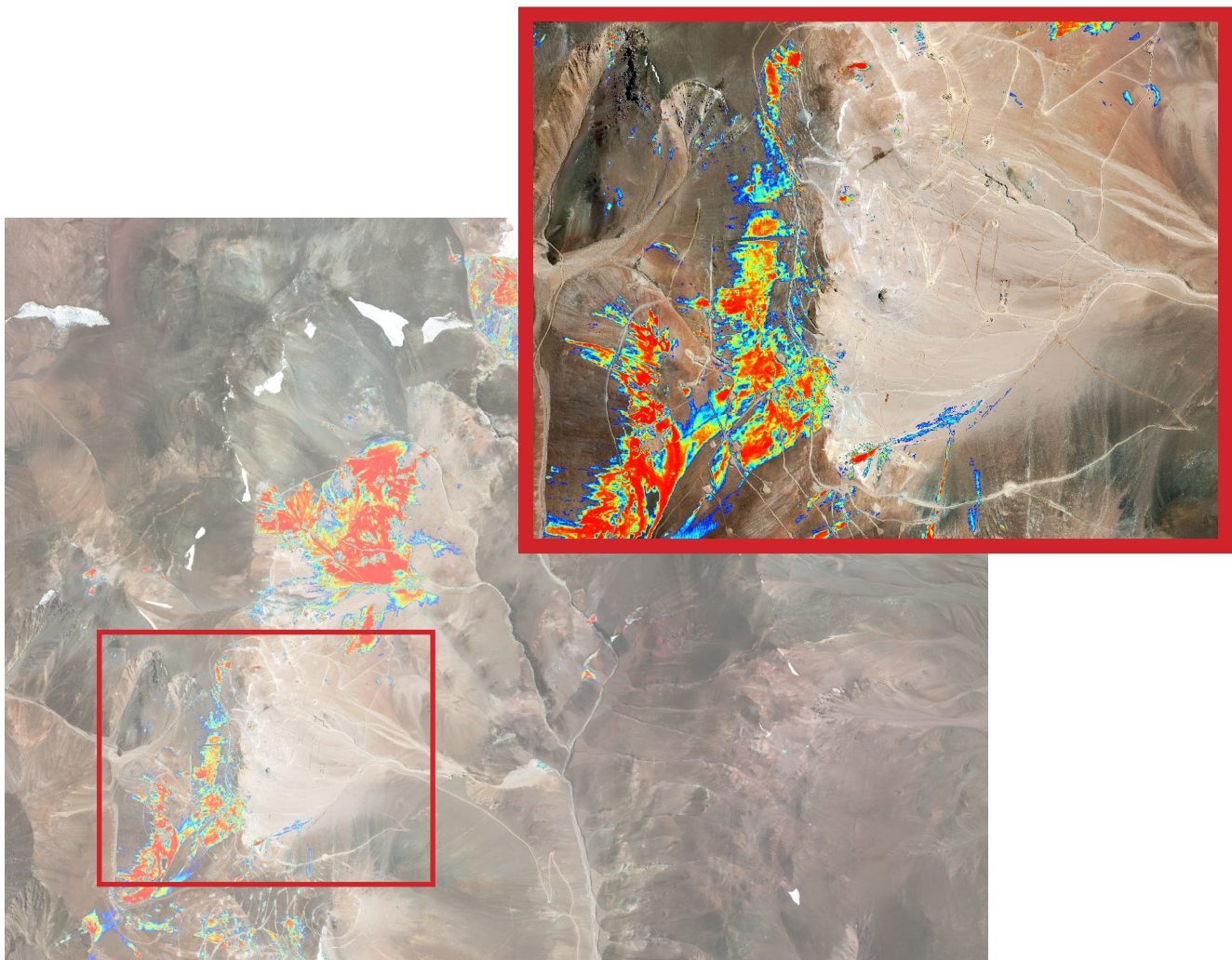


Figure 2: Close-up of kaolinite at the Filo del Sol Zone

Methods

Launched in 2019, our current alteration mineral mapping process is an application of spectral analysis to satellite imagery, using proprietary data processing with deep learning technology.

PhotoSat works with either WorldView-3 (WV-3) or ASTER satellite imagery. Since WV-3 has been operational since 2014, archive imagery is available, and it is also

possible to task the satellite for new satellite imagery.

Spectral Resolution

WV-3 is equipped with multispectral imaging instruments capable of collecting information from 16 sensor bands.

With WV-3, these bands cover specific wavelengths of the visible and near-infrared (VNIR) and SWIR parts of the electromagnetic (EM) spectrum (Fig. 3).

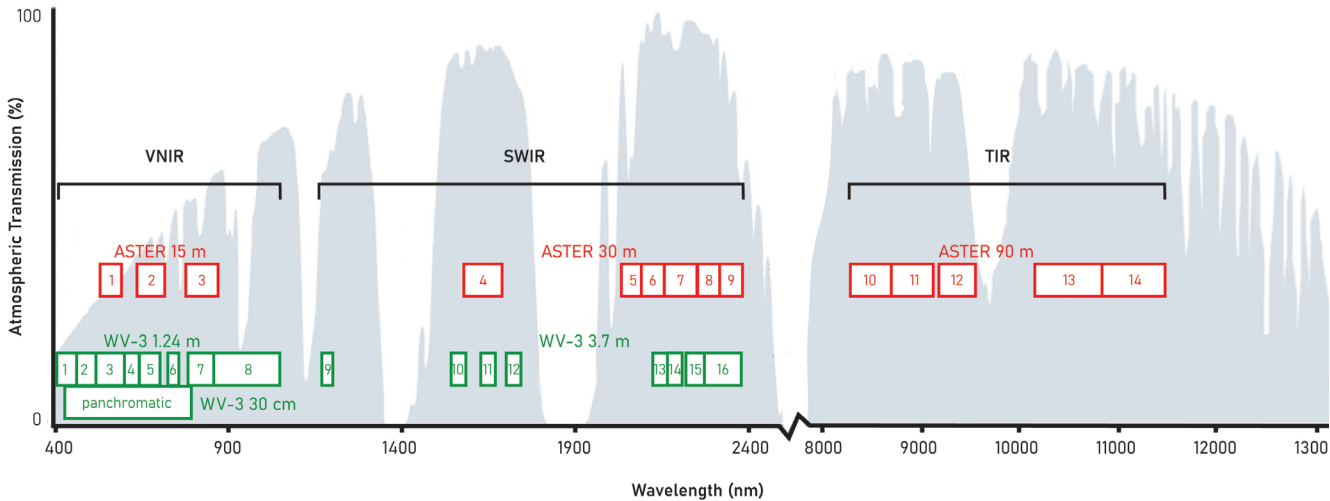


Figure 3: Bands detected by WV-3 and ASTER

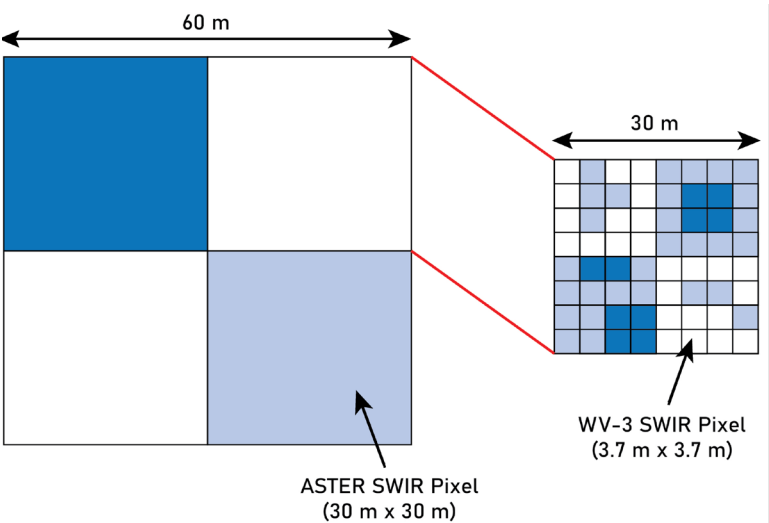


Figure 4: SWIR pixel size of WV-3 and ASTER

Spatial Resolution

WV-3 satellite imagery is high-resolution with a VNIR pixel size of 1.2 m and a SWIR pixel size of 3.7 m.

Because of its small pixel sizes, WV-3 imagery provides a high level of detail. It is suitable for alteration mapping at both regional and property scale.

Spectral Matching

Minerals have unique spectral characteristics that can be used to identify them. To positively identify a mineral, we look for and examine diagnostic features in the spectral profile or “signature”.

Slope

Changes in slope between spectral bands can be used to identify some minerals. Not all slopes are distinct from each other, so the slope alone may be insufficient as a means of identification.

Absorption Features

Minerals have unique absorption features in their spectral signature, which appear as dips in the profile.

The spectral profile of each pixel in a satellite image can be matched or compared to reference spectral profiles of known minerals and other surface materials using resources such as the USGS Spectral Library (Fig. 5).

PhotoSat maintains an internal library of reference spectral profiles for this purpose, collected from a variety of sources.

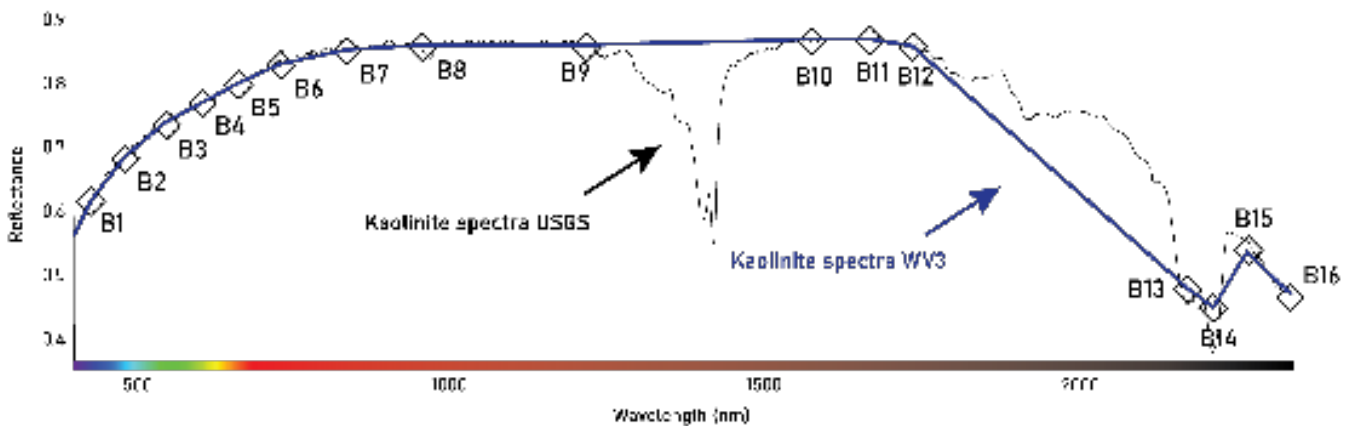


Figure 5a: Spectral profile of kaolinite with WV-3

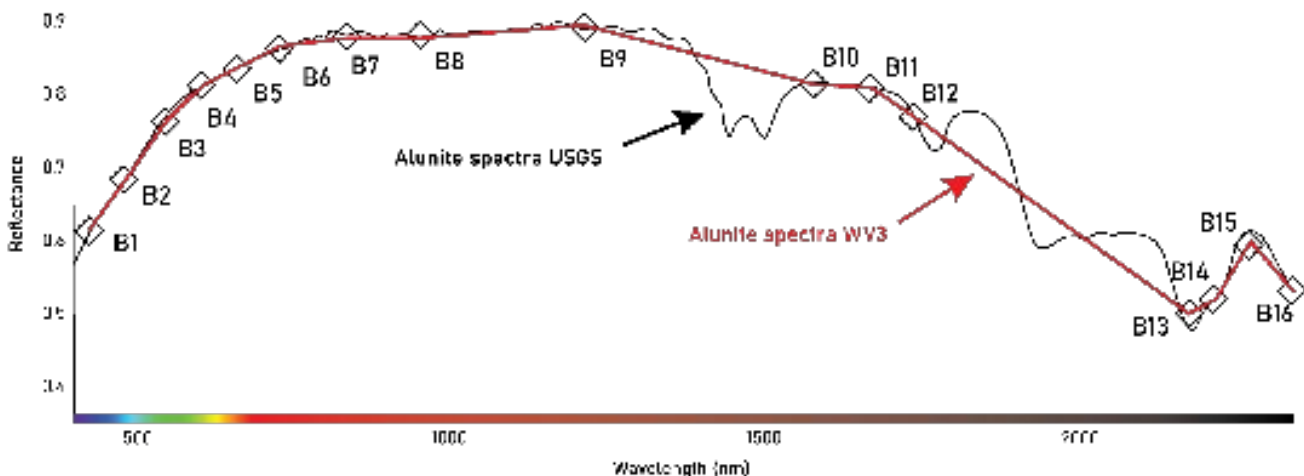


Figure 5b: Spectral profile of alunite with WV-3

Deep Learning

PhotoSat uses deep learning technology in its data processing.

Reliability and Repeatability

PhotoSat's data processing is governed by proprietary algorithms which create repeatable results.

This consistency applies to alteration mapping at property scale, and also between alteration projects that are located in different regions.

CNN Training

In alteration mapping, the use of convolutional neural networks (CNN) allows for continual improvement of the process.

By conducting alteration mapping tests in areas rich in surficial data, we can train the CNN, therefore improving future performance and assessing the reliability of our current alteration mapping processes.



Results

This report includes a separate alteration image for each mineral detected. These are shown in Figure 7 to Figure 22.

Natural Colour

This orthophoto (Fig. 6) shows the area around the Filo del Sol deposit in natural colour.

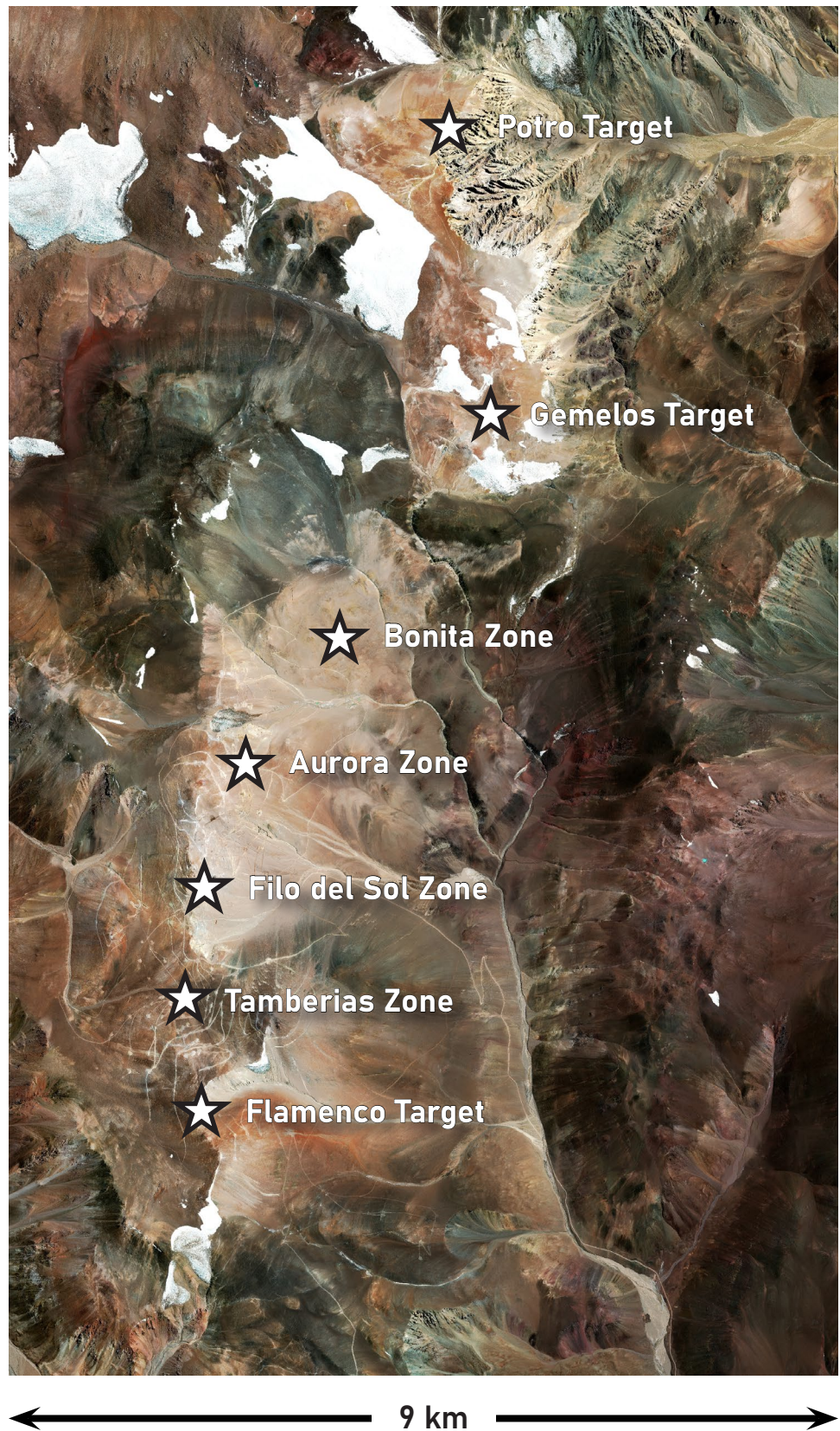


Figure 6: Natural colour image of the Filo del Sol deposit

Geology Enhanced Colour

This geology enhanced image (Fig. 7) shows the area around the Filo del Sol deposit.

Geology enhanced images are produced by combining two VNIR bands and one SWIR band. They accentuate additional surface details that are not visible in a regular orthophoto.

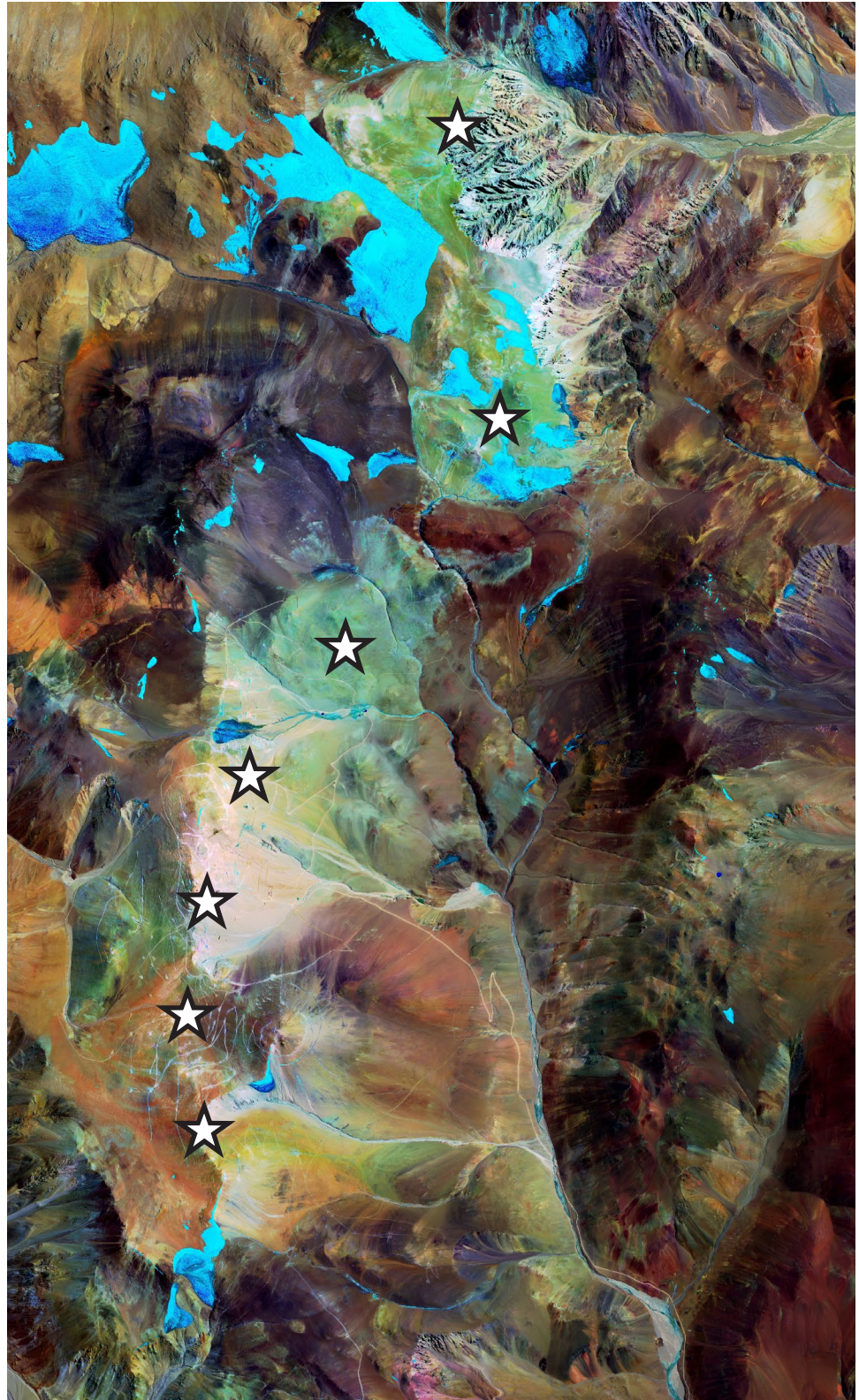


Figure 7: Geology enhanced image of the Filo del Sol deposit

Alunite

This alteration mineral map (Fig. 8) for alunite was produced from 16-band WV-3 satellite imagery at a pixel size of 2 m.

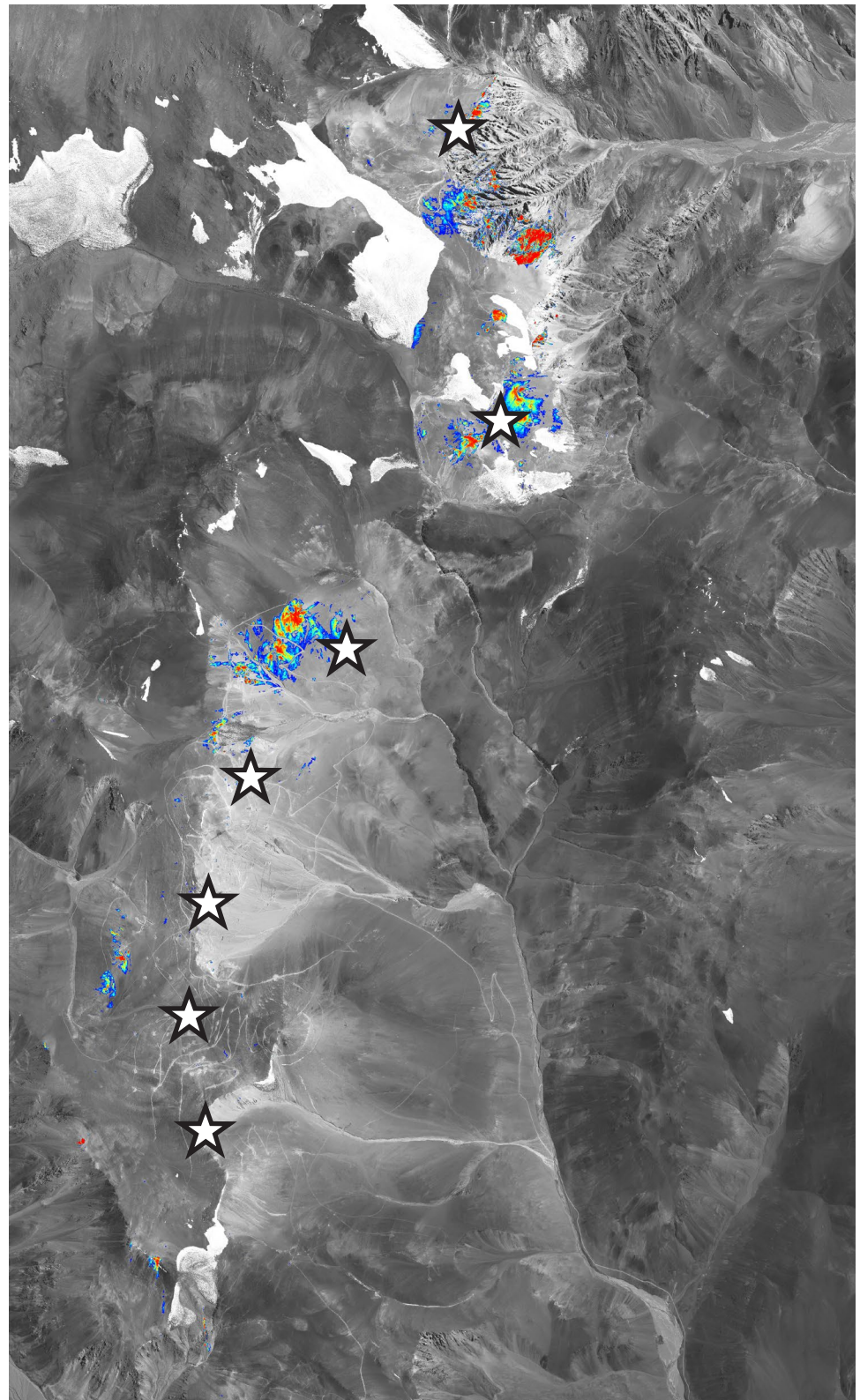
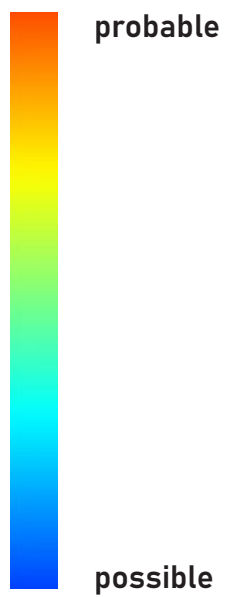


Figure 8: Alteration map of alunite with WV-3 imagery

Kaolinite

This alteration mineral map (Fig. 9) for kaolinite was produced from 16-band WV-3 satellite imagery at a pixel size of 2 m.

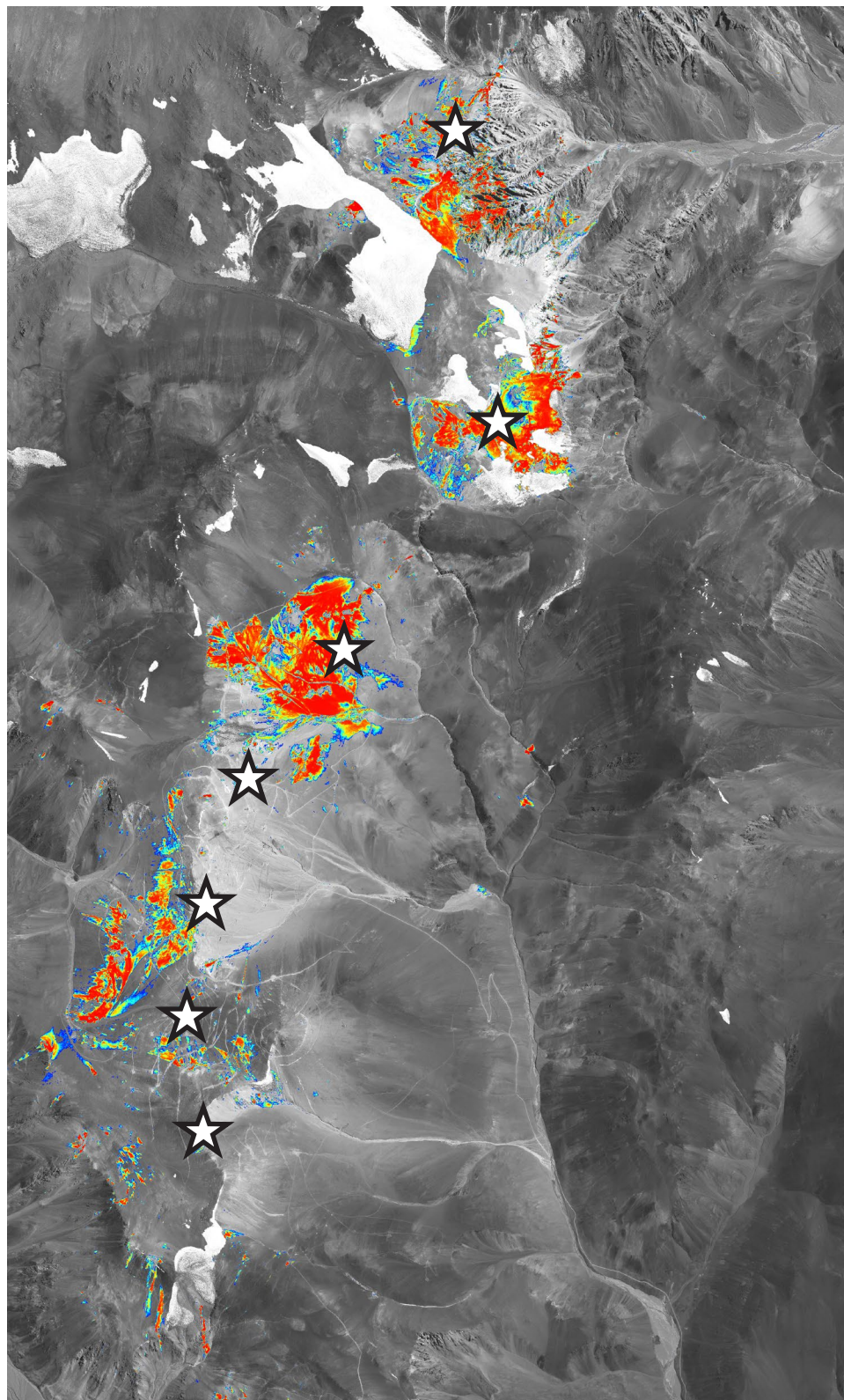
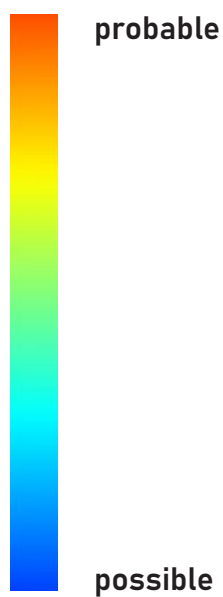
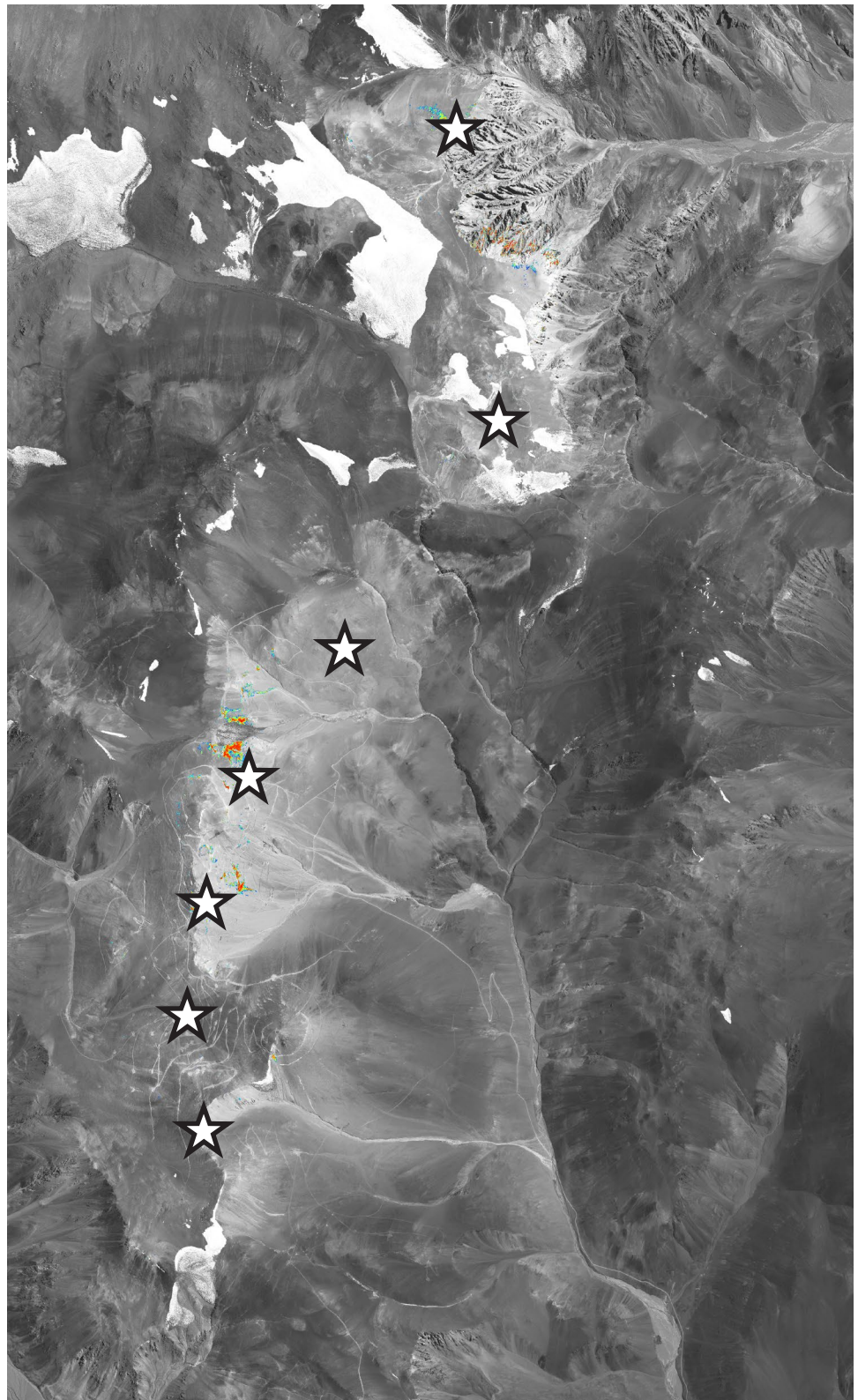
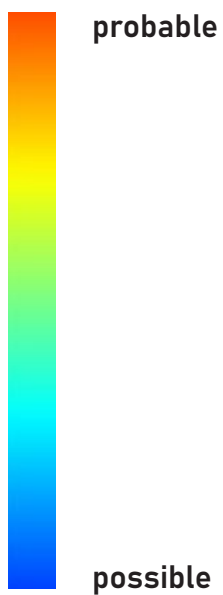


Figure 9: Alteration map of kaolinite with WV-3 imagery

Buddingtonite

This alteration mineral map (Fig. 10) for buddingtonite was produced from 16-band WV-3 satellite imagery at a pixel size of 2 m.

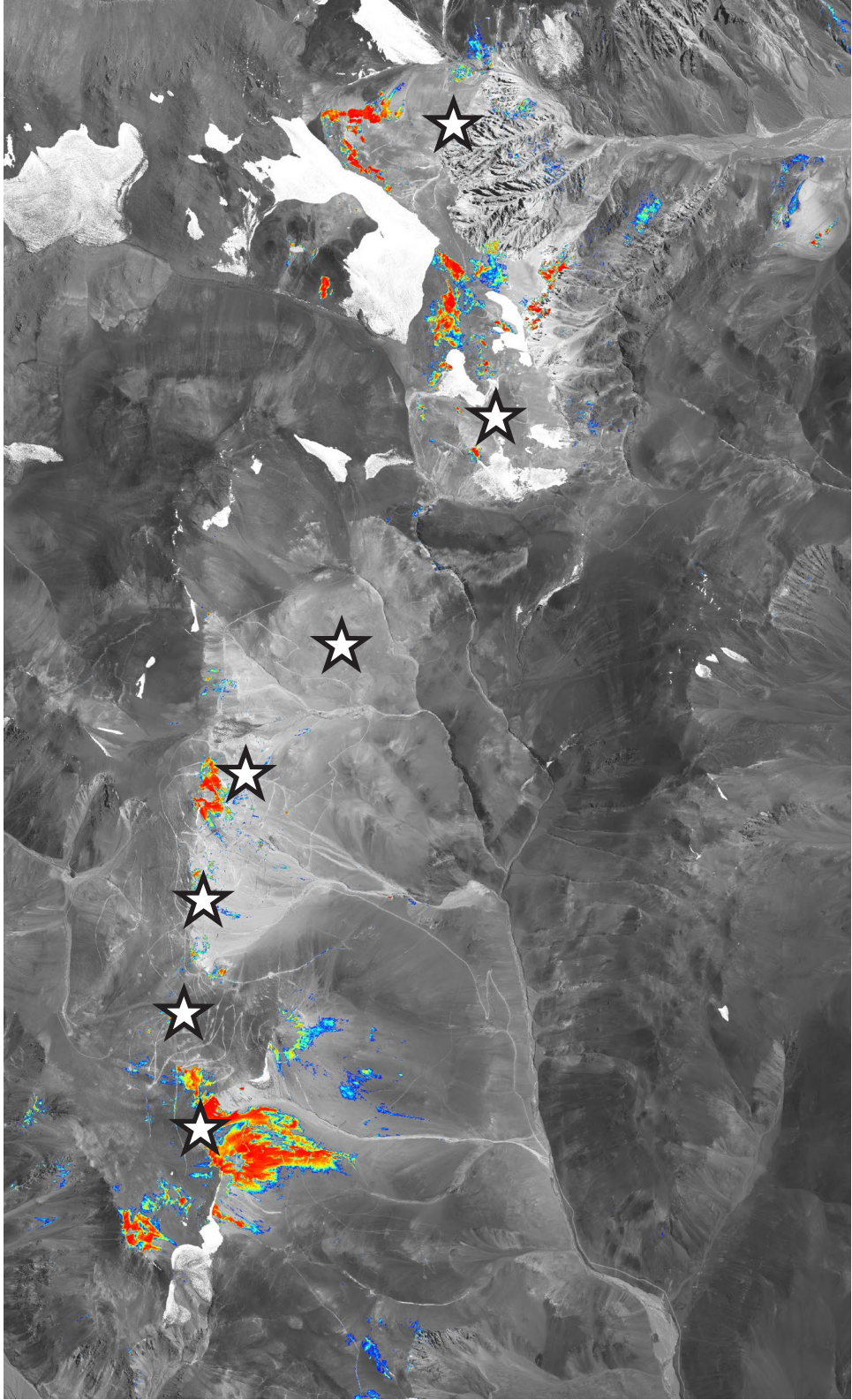
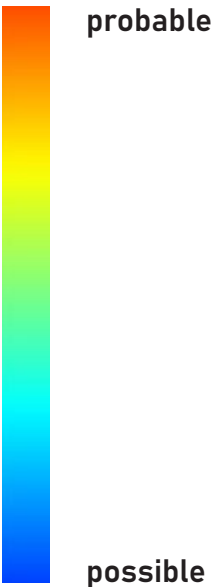


← 9 km →

Figure 10: Alteration map of buddingtonite with WV-3 imagery

Opal

This alteration mineral map (Fig. 11) for opal was produced from 16-band WV-3 satellite imagery at a pixel size of 2 m.

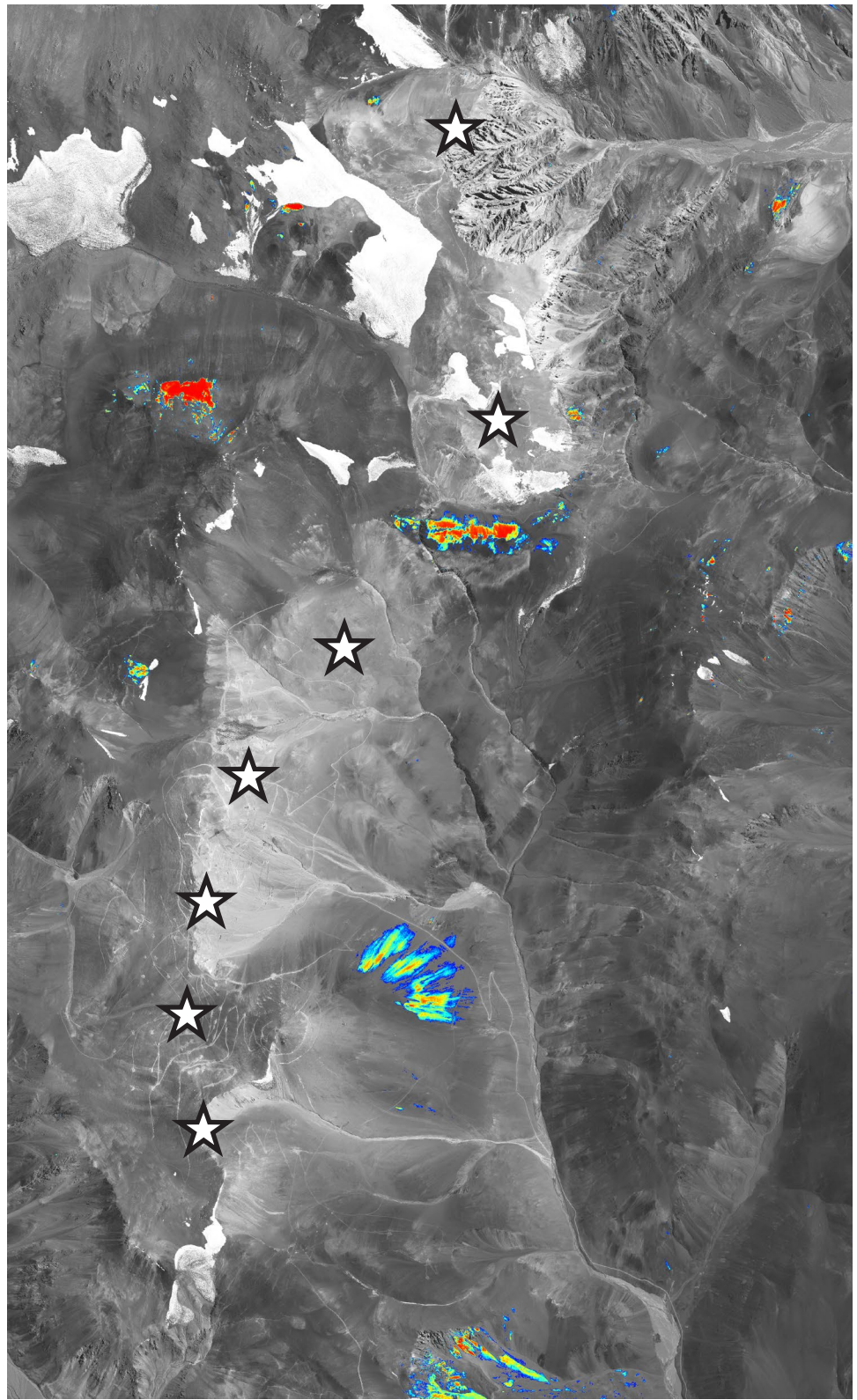
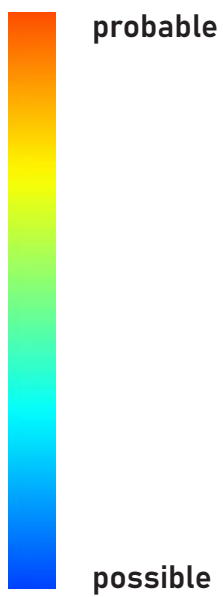


9 km

Figure 11: Alteration map of opal/chalcedony with WV-3 imagery

Calcite

This alteration mineral map (Fig. 12) for calcite was produced from 16-band WV-3 satellite imagery at a pixel size of 2 m.

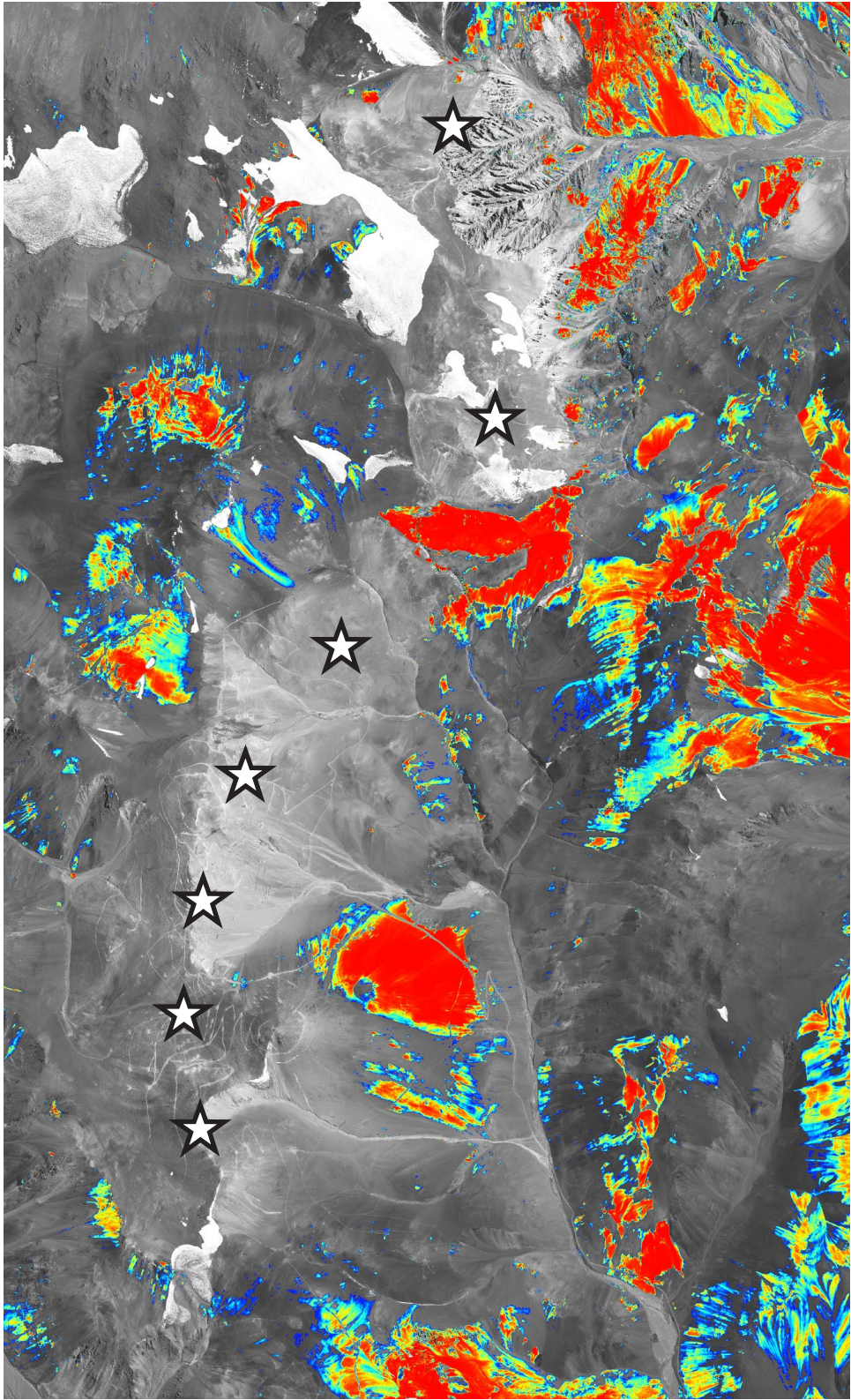
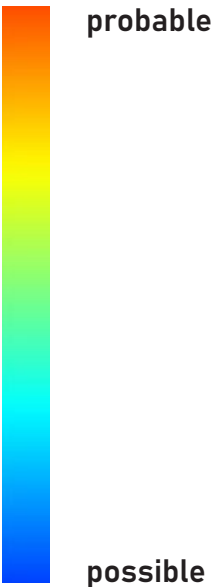


← 9 km →

Figure 12: Alteration map of calcite with WV-3 imagery

Chlorite

This alteration mineral map (Fig. 13) for chlorite was produced from 16-band WV-3 satellite imagery at a pixel size of 2 m.



9 km

Figure 13: Alteration map of chlorite/epidote with WV-3 imagery

Sericite

This alteration mineral map (Fig. 14) for sericite was produced from 16-band WV-3 satellite imagery at a pixel size of 2 m.

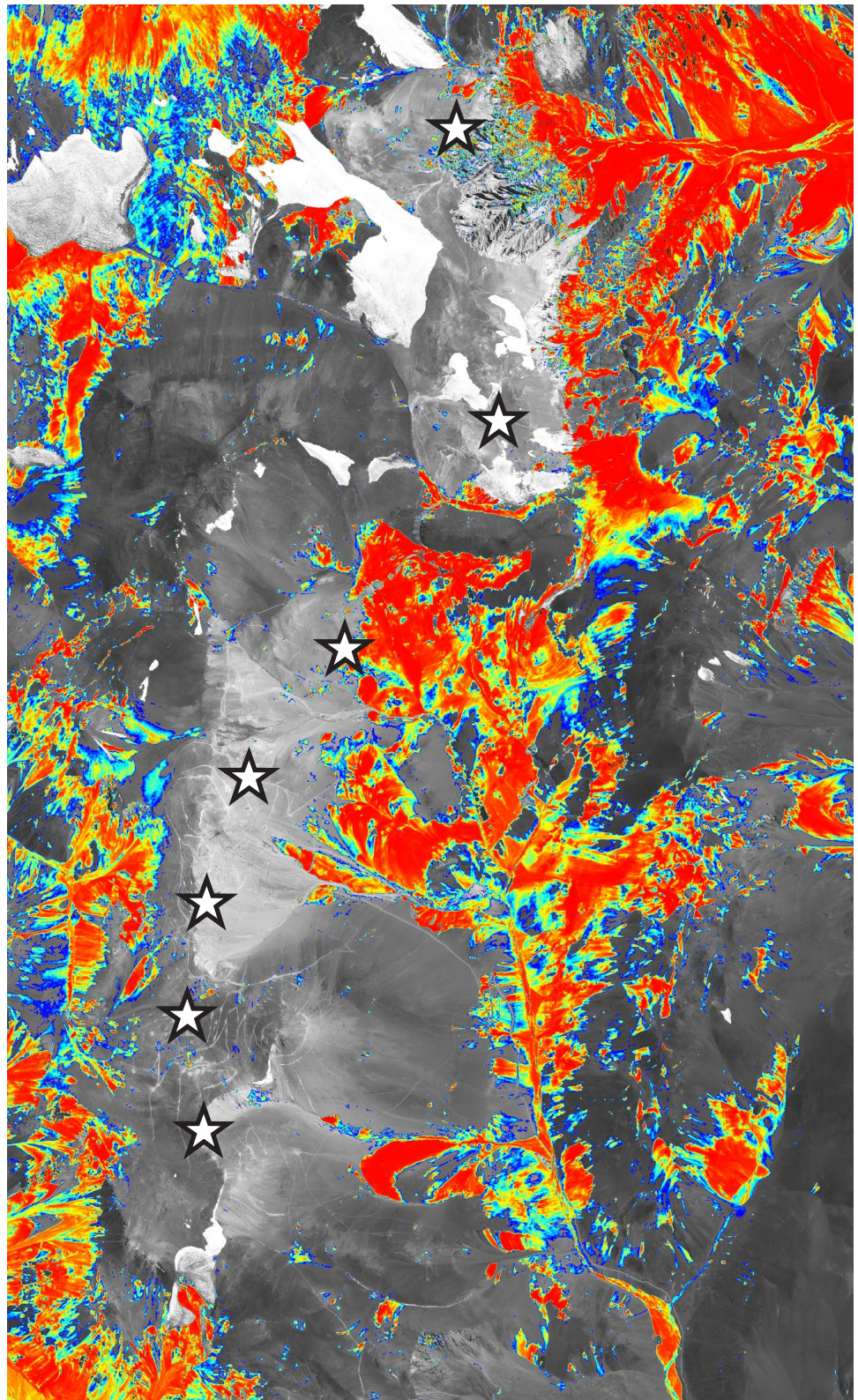
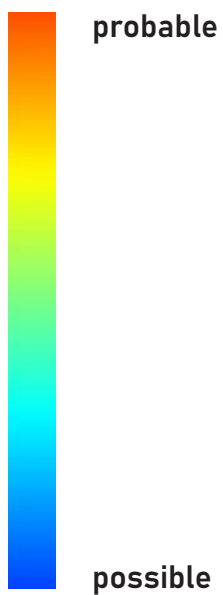
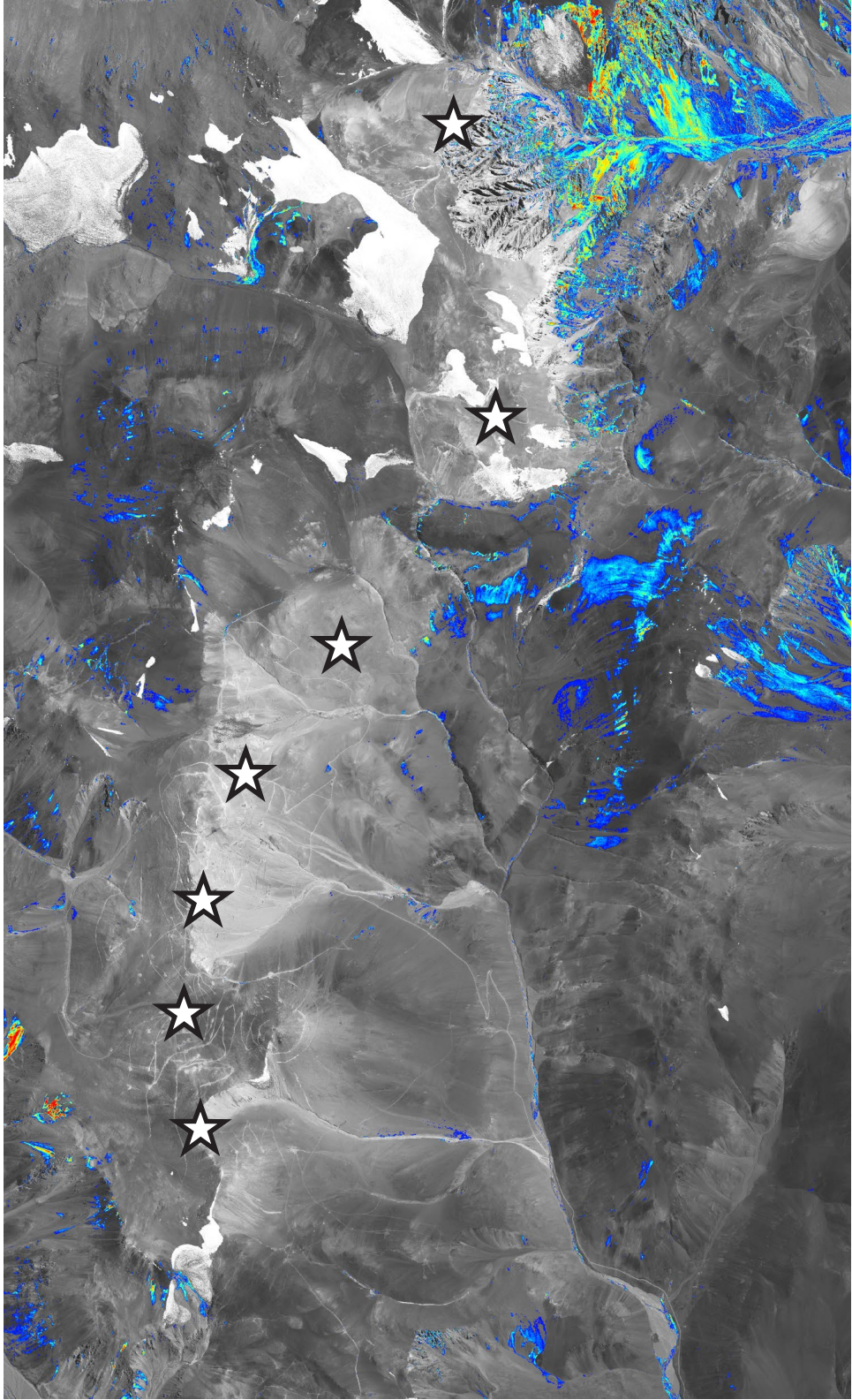


Figure 14: Alteration map of sericite with WV-3 imagery

Montmorillonite

This alteration mineral map (Fig. 15) for montmorillonite was produced from 16-band WV-3 satellite imagery at a pixel size of 2 m.

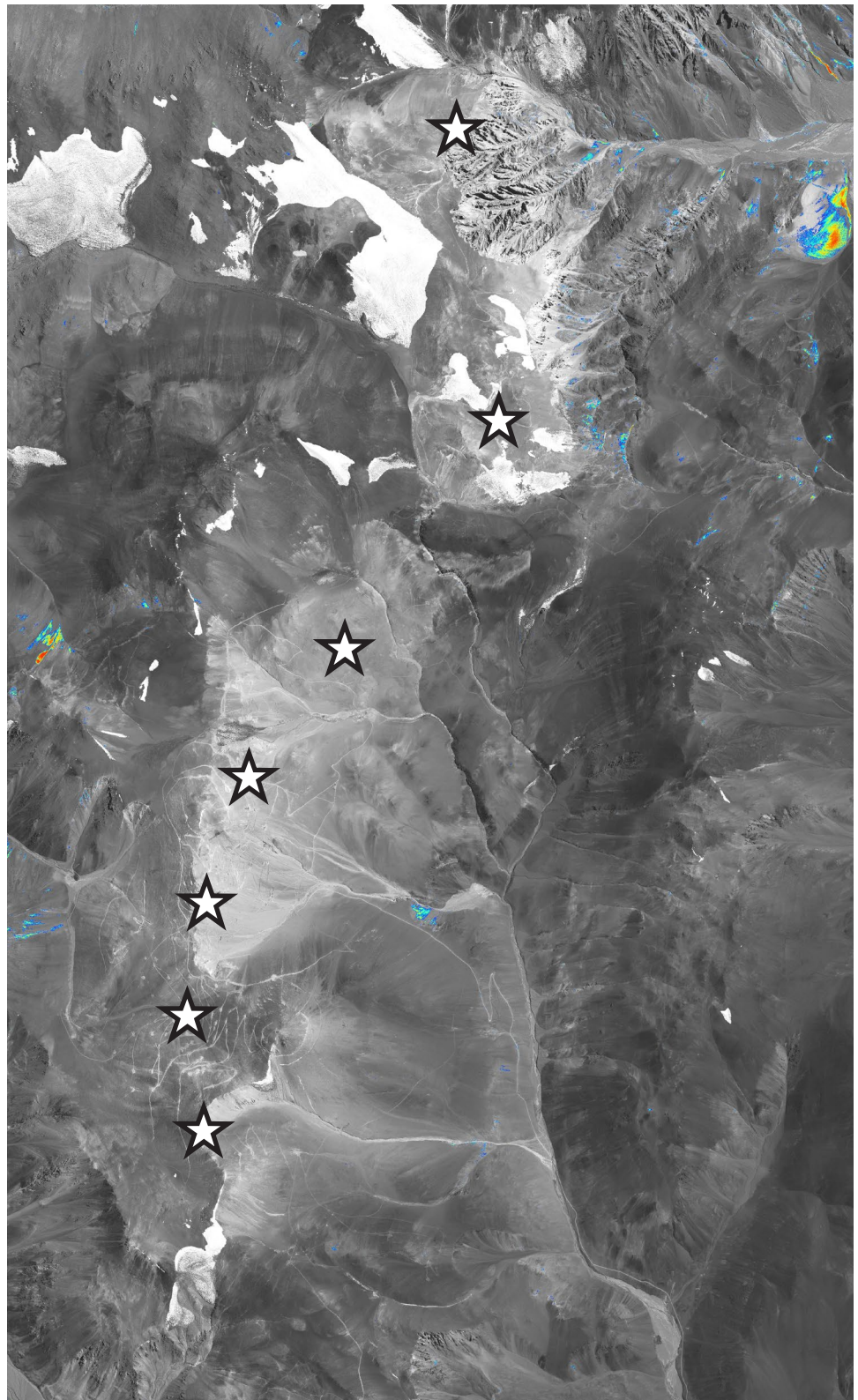
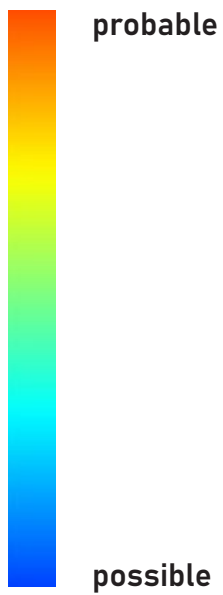


9 km

Figure 15: Alteration map of montmorillonite with WV-3 imagery

Goethite

This alteration mineral map (Fig. 16) for goethite was produced from 16-band WV-3 satellite imagery at a pixel size of 2 m.



← 9 km →

Figure 16: Alteration map of goethite with WV-3 imagery

Hematite

This alteration mineral map (Fig. 17) for hematite was produced from 16-band WV-3 satellite imagery at a pixel size of 2 m.

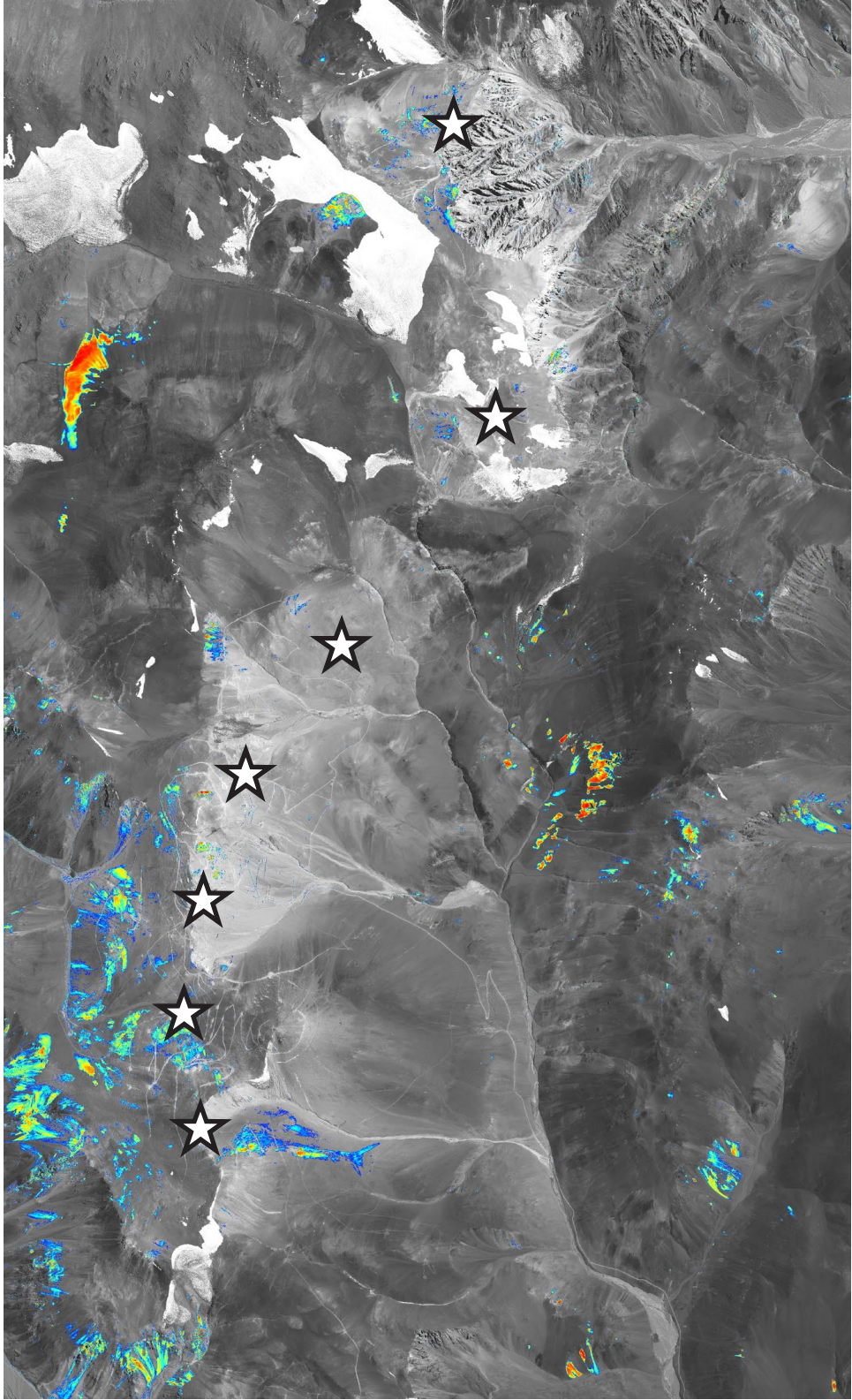


Figure 17: Alteration map of hematite with WV-3 imagery

Jarosite

This alteration mineral map (Fig. 18) for jarosite was produced from 16-band WV-3 satellite imagery at a pixel size of 2 m.

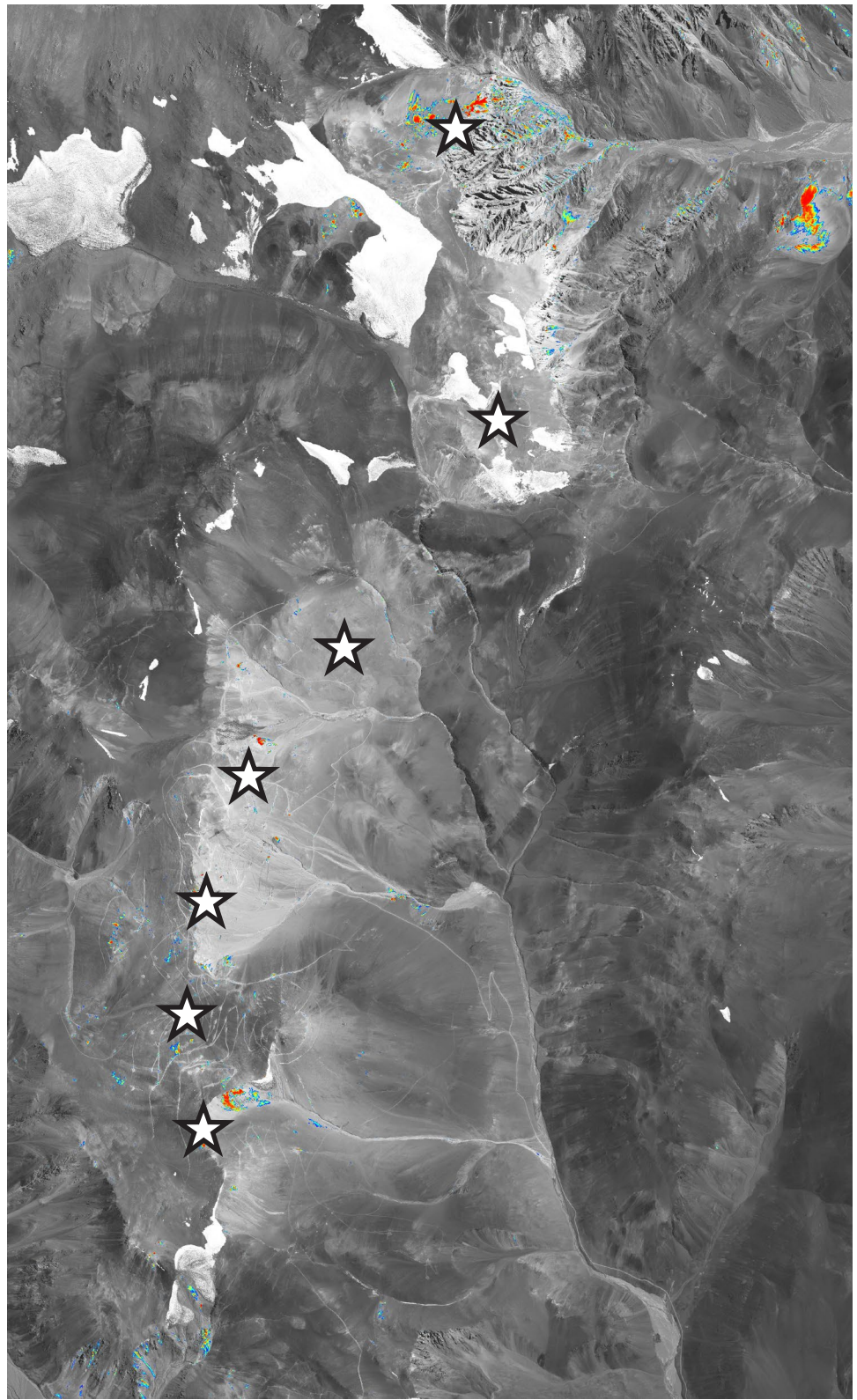


Figure 18: Alteration map of jarosite with WV-3 imagery

Iron Oxide Gossans

This alteration mineral map (Fig. 19) for iron oxide gossans was produced from 16-band WV-3 satellite imagery at a pixel size of 2 m.

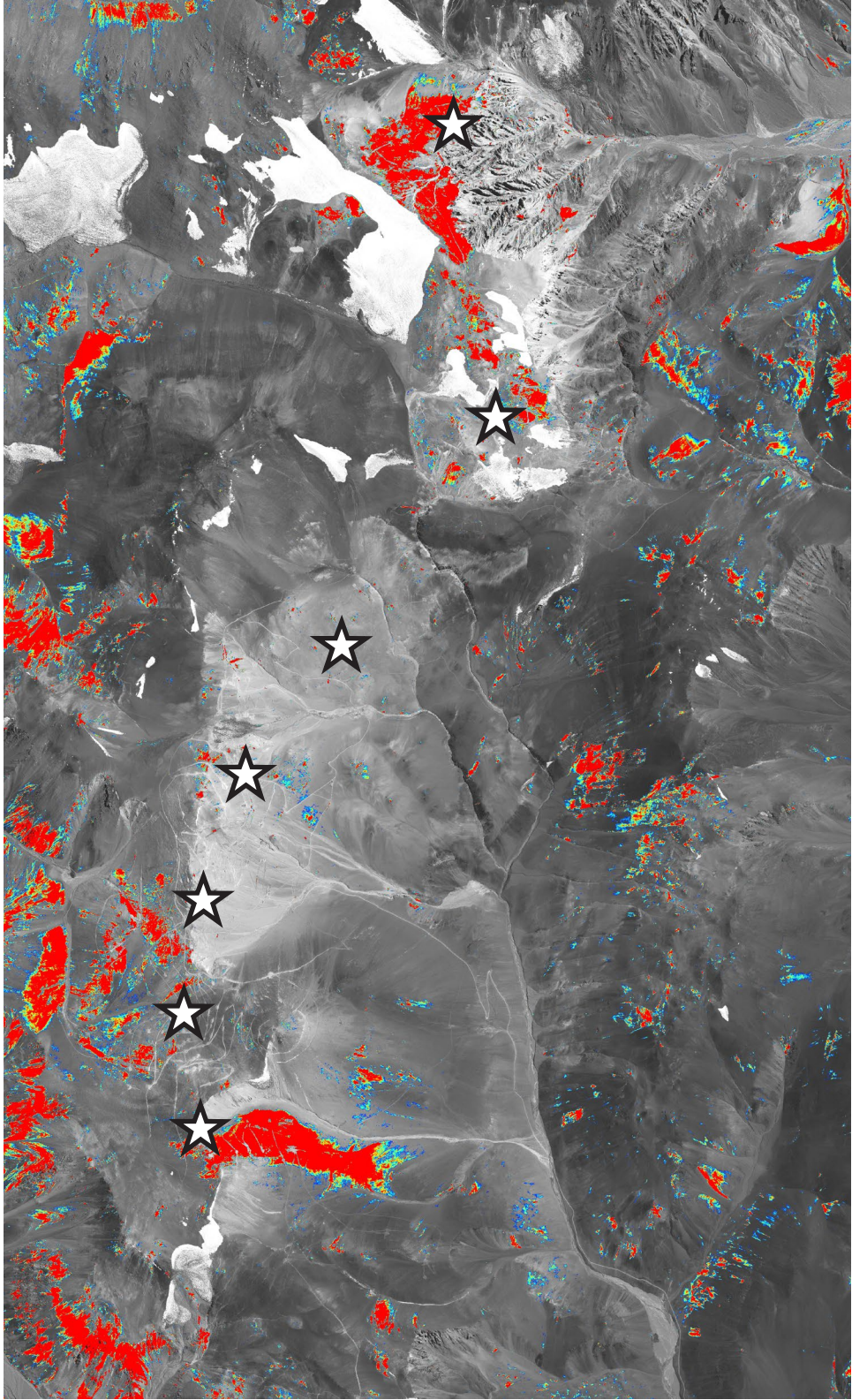
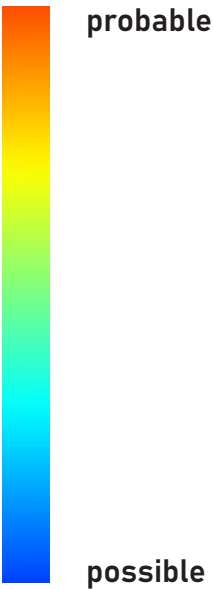


Figure 19: Alteration map of iron oxide gossans with WV-3 imagery

Silica

This alteration mineral map (Fig. 20) for silica was produced from 14-band ASTER satellite imagery at a pixel size of 75 m.

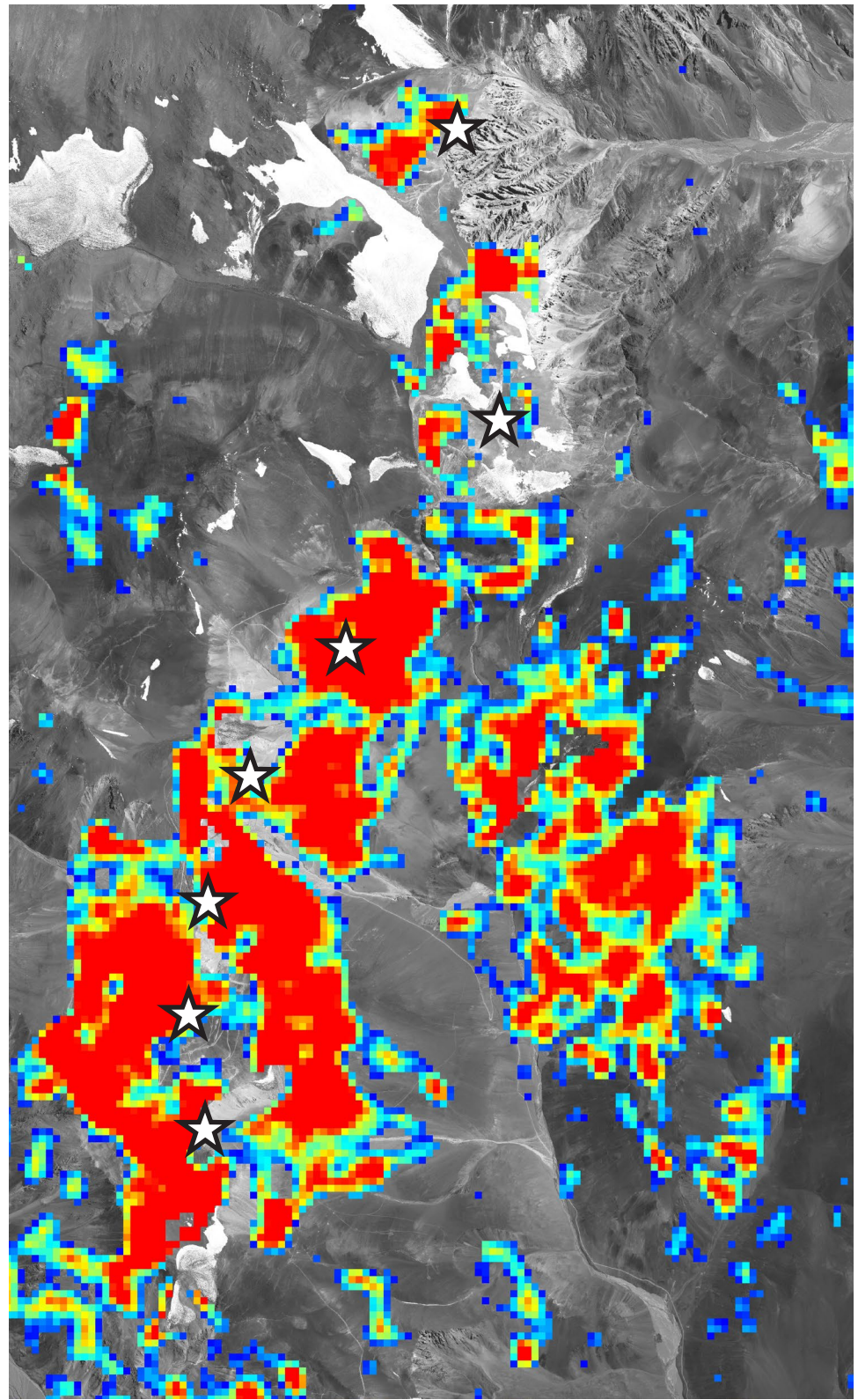
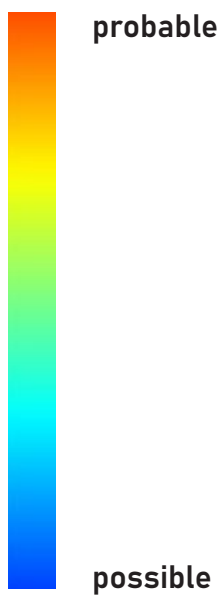
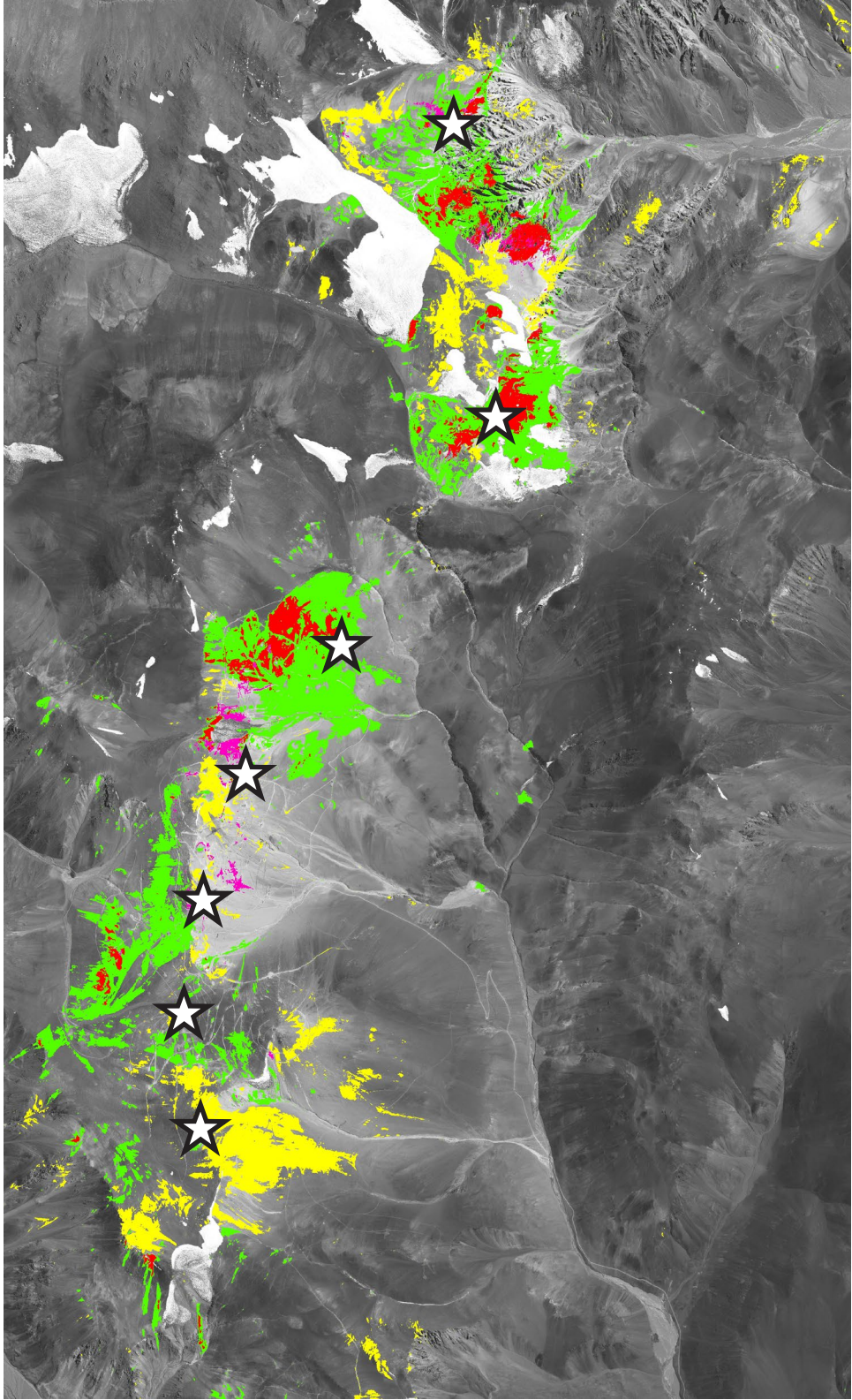


Figure 20: Alteration map of silica (75 m) from ASTER imagery

Clays and Other Minerals

This compilation map (Fig. 21) shows several alteration minerals around the Filo del Sol deposit.

-  Alunite
-  Kaolinite
-  Buddingtonite
-  Opal



← 9 km →

Figure 21: Compilation map of clays and other minerals

Micas, Clays, and Other Minerals

This compilation (Fig. 22) shows several alteration minerals around the Filo del Sol deposit.

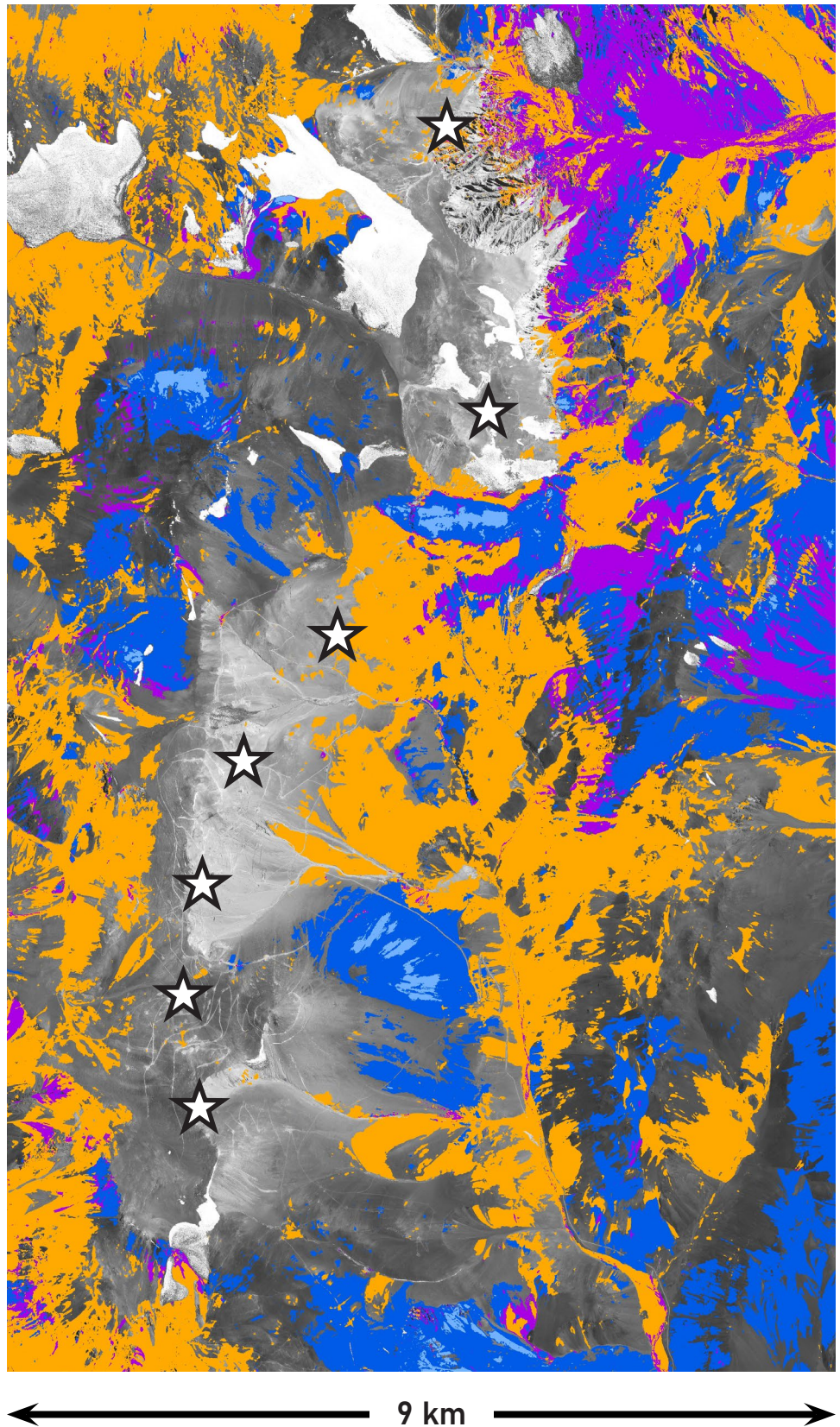
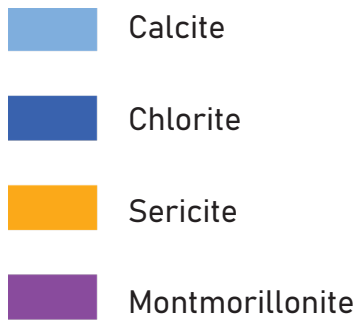
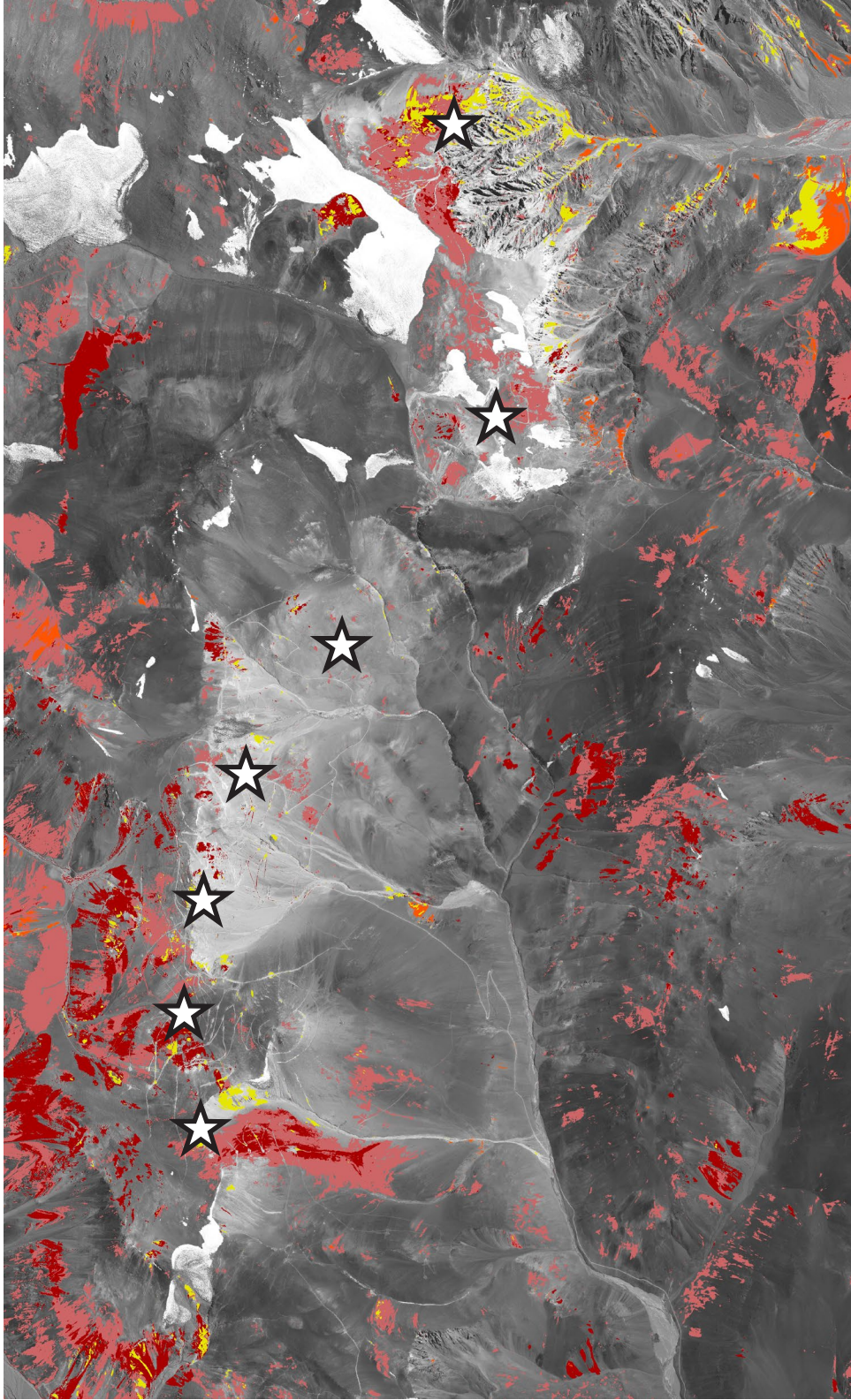


Figure 22: Compilation map of micas, clays, and other minerals

Iron Minerals

This compilation (Fig. 23) shows iron-containing alteration minerals around the Filo del Sol deposit.

-  Goethite
-  Hematite
-  Jarosite
-  Iron oxide



← 9 km →

Figure 23: Compilation map of iron minerals

Discussion

From testing, we know that certain alteration minerals can be reliably mapped through PhotoSat's data processing with deep learning technology.

If alteration is present at surface and visible in satellite photos, PhotoSat's alteration mineral mapping produced from WV-3 satellite imagery can detect the following minerals:

Micas

The result for sericite, or white mica, may consist of one or some combination of:

- **Muscovite:** $KAl_2(Si_3Al)O_{10}(OH,F)_2$
- **Paragonite:** $NaAl_2[(OH)_2AlSi_3O_{10}]$
- **Illite:** $(K,H_3O)(Al,Mg,Fe)_2(Si,Al)_4O_{10}[(OH)_2,(H_2O)]$

Iron Minerals

PhotoSat can identify:

- **Iron Oxide Gossans:** many different red, orange, and brown iron oxide minerals.
- **Hematite:** $Fe^{3+}_2O_3$
- **Goethite:** $Fe^{3+}O(OH)$
- **Jarosite:** $KFe^{3+}_3(SO_4)_2(OH)_6$

Clay Minerals

PhotoSat can identify:

- **Alunite:** $(Na,K)Al_3(SO_4)_2(OH)_6$
- **Kaolinite:** $Al_2Si_2O_5(OH)_4$
- **Montmorillonite:** $Na,Ca)_{0,3}(Al,Mg)_2Si_4O_{10}(OH)_2 \cdot n(H_2O)$

*PhotoSat cannot differentiate between opal and chalcedony with 16-band WorldView-3.

**PhotoSat cannot differentiate between chlorite and epidote with 16-band WorldView-3.

Other Minerals

PhotoSat can identify:

- **Opal/Chalcedony*:** $SiO_2 \cdot nH_2O$
- **Buddingtonite:** $NH_4AlSi_3O_8$
- **Calcite:** $CaCO_3$
- **Chlorite/Epidote****
 $(Mg,Fe,Li)_6AlSi_3O_{10}(OH)_8 / Ca_2(Al,Fe)_2(SiO_4)(OH)_2$

Context Images

PhotoSat also includes the following images with its WV-3 alteration mapping package:

- 2 m Geology enhanced colour image
- 2 m Vegetation intensity
- 50 cm Colour orthophoto
- 50 cm Greyscale orthophoto